The electronic structures of $LaSn_3$ and $LaIn_3$

1989 J. Phys.: Condens. Matter 1 2677

(http://iopscience.iop.org/0953-8984/1/16/003)

J. Phys.: Condens. Matter 1 (1989) 2677–2682. Printed in the UK

The electronic structures of $LaSn_3$ and $LaIn_3$

Tang Shao-ping†, Zhang Kai-ming‡ and Xie Xi-de†

† China Centre of Advanced Science and Technology (World Laboratory), PO Box 8730, Beijing, and Department of Physics, Fudan University, Shanghai, People's Republic of China

‡ Department of Physics, Fudan University, Shanghai, People's Republic of China

Received 9 August 1988, in final form 18 November 1988

Abstract. We have performed LMTO ASA calculations of the electronic structures of LaM_3 ($M \equiv Sn$, In). It is shown that the interactions between La d and Sn or In p states are the main bonding states in LaM_3, therefore indicating that LaM_3 behaves like a transition-metal compound. The differences between the electronic structures of LaM_3 and CeM_3 are discussed. The lattice constants and bulk modulus of LaM_3 are also calculated and compared with experimental values.

1. Introduction

The LaX_3 inter-metallic compounds (where $X \equiv Sn$, In, Tl or Pb) and their alloys have been the subject of many experimental and theoretical investigations. They are all superconducting materials and some exhibit coexistence of a relatively high superconducting transition temperature T_c and a large temperature-dependent paramagnetic susceptibility χ [1]. These systems also show that the superconductive critical temperature T_c follows a W-shaped curve if plotted as a function of the valence electron concentration n [2]. In addition, a study of the electronic structure of LaX_3 could be helpful to the understanding of the anomalous behaviour of some isostructural Ce compounds (e.g. $CeSn_3$) and their alloys.

Recently, in [3] an electronic structure calculation for CeM_3 (where $M \equiv Sn$ on In) was carried out with the linearised muffin-tin orbital (LMTO) method. Reasonable descriptions of the itinerancy of f electrons in CeM_3 were given. It was shown that the f electrons in CeM_3 play an important role in determining the energy band structure, the density of states etc. The f-electron itinerancy is responsible in part for many intriguing physical phenomena, e.g. the mixed valence. To understand in detail the differences between the electronic structures of LaM_3 and CeM_3 using the same theoretical method, in this paper, we present a self-consistent LMTO calculation of LaM_3.

The electronic structures of LaM_3 have been studied by a number of researchers. In [4] the band structure of $LaSn_3$ was calculated with the orthogonal plane-wave method. At the same time, in [5] the band structures of $LaSn_3$ and $LaIn_3$ were obtained with the augmented plane-wave (APW) method. In [6] the Fermi surface calculation of $LaSn_3$ was carried out with the linearised APW (LAPW) method. In [7] the cohesive properties and electronic structure of $LaIn_3$ were calculated with the augmented spherical-wave (ASW) method; in this calculation, relativistic effects and the f orbital of La were not included.

0953-8984/89/162677 + 06 $02.50

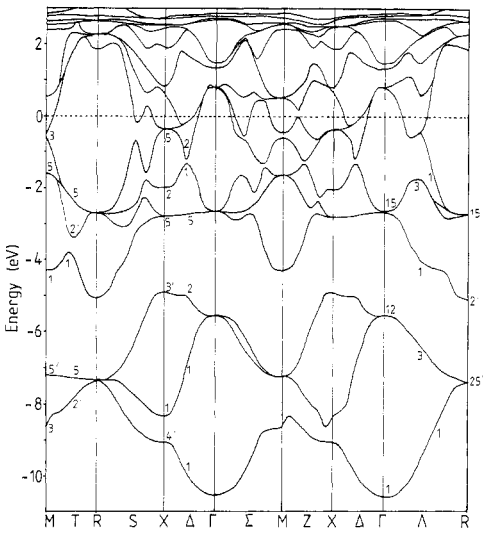

Figure 1. The energy band structure of $LaSn_3$. The Fermi energy is chosen as the energy zero.

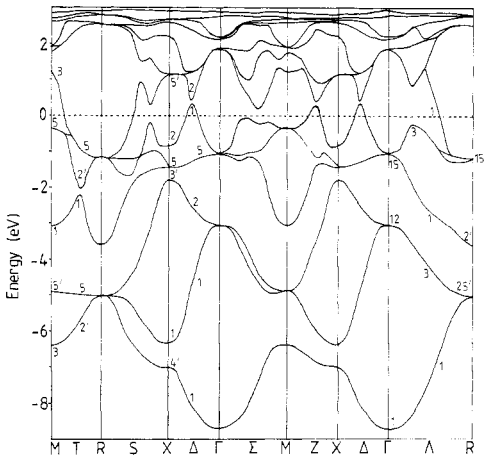

Figure 2. The energy band structure of $LaIn_3$.

2. Details of the calculation

We use the semi-relativistic version [8] of the LMTO method as was used [3] to describe the electronic structure of CeM_3. The core states are recalculated fully relativistically during each iteration, while the valence states are treated in a semi-relativistic way, i.e. the spin–orbit coupling is omitted in solving the Dirac equation. The interpolation formula in [9] is used for the exchange–correlation potential. The maximal angular momentum l_{max} was chosen to be $l_{max} = 3$ for La and $l_{max} = 2$ for Sn and In.

LaM_3 crystallises in the $AuCu_3$ structure; the lattice constants of $LaSn_3$ and $LaIn_3$ are 4.769 Å and 4.735 Å [10], respectively. In our calculation, the 24 special k-points [11] are used for the Brillouin zone integration and the final density of states (DOS) is obtained from 56 k-points.

3. Results and discussion

3.1. The energy band structure and Fermi surface

Figure 1 shows the band structure of $LaSn_3$. The lower three valence bands are mainly of Sn s character. The bands near E_F consist of the Sn p and La d hybridisation states. There are three bands intersecting with the Fermi energy. The seventh band is almost an occupied band; it crosses Fermi energy near the Γ point. The eighth band has a band width of 2.5 eV; it oscillates and intersects more steeply with E_F. This is a light-mass band and contributes more to conductivity.

The band structure of $LaSn_3$ differs from that of $CeSn_3$ [3] near E_F. In $CeSn_3$, the width of the eighth band is about 1.3 eV and the ninth band intersects E_F several times. In $LaSn_3$, the dispersion of the eighth band is larger. The ninth band intersects E_F only along the Δ direction.

The band structure of $LaIn_3$ is displayed in figure 2. On comparison with the band structure of $LaSn_3$, it can be seen that the width of the whole valence band of $LaIn_3$ is

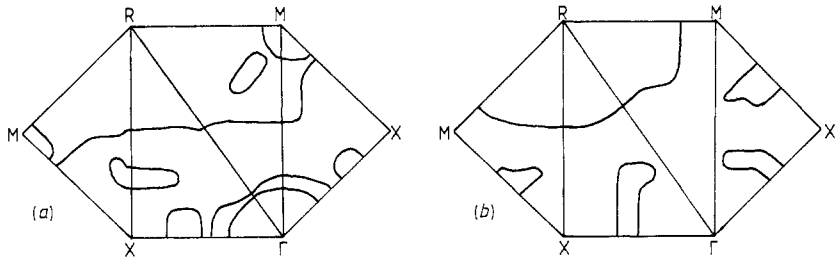

Figure 3. Intersection of Fermi surface of (*a*) $LaSn_3$ and (*b*) $LaIn_3$ with the high-symmetry planes of the Brillouin zone.

smaller than that of $LaSn_3$. In $LaIn_3$, there are two bands intersecting E_F, i.e. the sixth and seventh bands. The seventh band has a larger dispersion and is a light-mass band. In $CeIn_3$ [3], only the seventh band crosses E_F; so the Fermi surface of $CeIn_3$ will be simpler than that of $LaIn_3$. In figure 3, we show the intersection of the Fermi surface of $LaSn_3$ and $LaIn_3$ in the high-symmetry planes of Brillouin zone. The Fermi surface of $LaSn_3$ is similar to figure 2 in [6], but our results have two more 'pockets' near the ΓX axis caused by the ninth band and no hole near the X point due to the eighth band. These differences might be caused by spin–orbit effects which have been omitted in our calculation. In [6], these effects were included in the final iteration of the self-consistent calculation. After detailed analysis of figure 1, it can be seen that the seventh and eighth bands are degenerate at the X point and the eighth and ninth bands degenerate partially along the ΓX line. If spin–orbit coupling is considered, the degenerate bands would split into two bands; when the higher band crosses E_F, the Fermi surface will become similar to that in [6].

The Fermi surface of $LaIn_3$ is relatively simple. Except for the large pocket near the R point which is generated by the seventh band, the rest of the Fermi surface is due to the sixth band.

3.2. The density of states

Figure 4 shows the total and *l*-projected density of states (DOS) of $LaSn_3$. The projected DOSs of La s and p states are not shown because of their small value in the given energy range. For the Sn d states, the maximum value of its projected DOS is 1.0 states eV^{-1}/cell) at 2.4 eV; in the other energy range, its value is less than 0.3 states eV^{-1}/cell). From figure 4, it can be seen that the general shape of the DOS curve is quite similar to that given by LAPW method [6]. The Sn p and La d hybridisation states contribute the total DOS between −4 eV and the Fermi energy, which indicates the major bonding states in $LaSn_3$. In $CeSn_3$ [3], however, the Ce 4f states have a large contribution to bonding [3]. The La 4f states at 2.6 eV are localised states, while the Ce 4f states are very close to E_F, showing the itinerant property.

Figure 5 shows the total DOS of $LaIn_3$. According to the projected DOS, the La d and In p hybridisation states contribute to the total DOS between −3 eV and E_F; this reflects the major bonding between La and In. Our results can be compared with the ASW calculation [7]. The agreement is good for those states below E_F; however, because the f orbitals are not considered in the ASW calculation, the DOS curve is quite different for states above E_F.

In table 1, we list values of the projected and total DOSs at the Fermi energy and the experimental values of the total DOS from specific heat measurements. The unenhanced

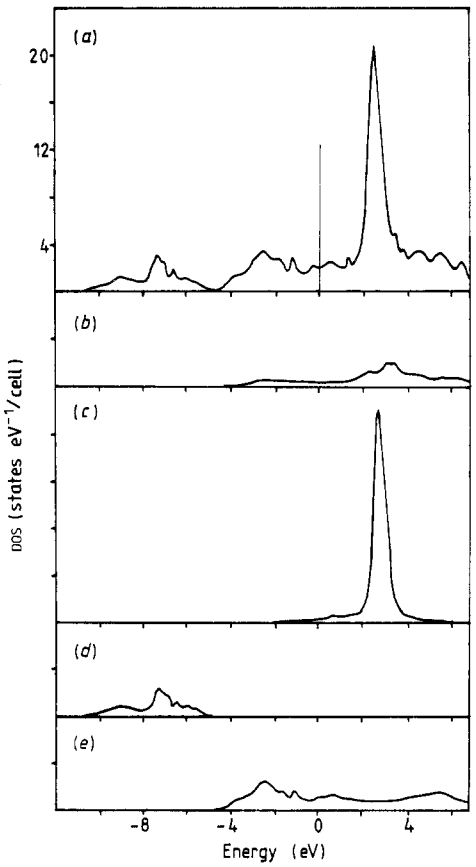

Figure 4. The total and *l*-projected DOSS of $LaSn_3$: (*a*) total $LaSn_3$; (*b*) La d; (*c*) La f; (*d*) Sn s, ×3; (*e*) Sn p, ×3.

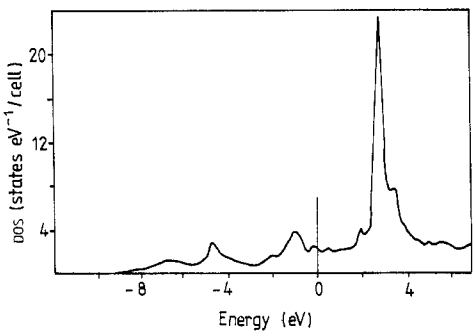

Figure 5. The total DOS of $LaIn_3$.

linear specific heat coefficient γ_0 is calculated from

$$\gamma_0 = \pi^2 k_B^2 N^{calc}/3. \tag{1}$$

The difference between the total DOS from experimental work and that from theoretical work is more than 4 states Ryd^{-1}/cell. In [7] it was considered that the discrepancy is due in part to neglecting the relativistic effects and the f state of La in the calculation. In the present work, we obtain a value of 25.7 states Ryd^{-1}/cell for the total DOS of $LaIn_3$, which is slightly improved compared with the ASW result of 23.4. So the discrepancy between theory and experiment is still to be resolved.

Table 1. Calculated total and *l*-projected DOSs at E_F.

	DOS (Ryd^{-1}/cell)			
	$LaSn_3$		$LaIn_3$	
	La	Sn	La	In
N(s)	0.42	1.72	0.52	2.15
N(p)	0.54	16.07	0.45	12.31
N(d)	3.99	3.51	5.96	2.48
N(f)	3.07	—	1.83	—
N^{tot}	29.32		25.70	
N^{exp} [12]	34.9		29.8	
γ_0 (mJ mol^{-1} K^{-2})	6.03		5.09	

Table 2. The equilibrium lattice constants a and bulk moduli B of $LaSn_3$ and $LaIn_3$.

	$LaSn_3$		$LaIn_3$	
	a (Å)	B (Mbar)	a (Å)	B (Mbar)
Present work	4.73	0.78	4.70	0.59
ASW calculation	—	—	4.925 [7]	0.73 [7]
Experiment	4.769 [10]	0.515 [18]	4.735 [10]	—

Although it is somewhat arbitrary to define charges inside Wigner–Seitz spheres, we can compare the charge transfers for a series of La compounds. In the present choice of Wigner–Seitz radius (the ratio R_{Sn}/R_{La} or R_{in}/R_{La} of the sphere radii is 0.95), as in CeM_3 [3], the charge will transfer from the rare-earth metal La to Sn or In. This agrees with the estimation of Pauling electron negativity (for La, Sn and In, the Pauling electron negativities are 1.1, 1.8 and 1.7, respectively).

The specific heat measurements for $LaSn_3$ [13–15] at low temperatures indicate that the specific heat varies linearly with temperature. The specific heat coefficient γ_{exp} is found to be relatively large ($\gamma_{exp} \simeq 11$ mJ mol^{-1} K^{-2}) which suggests that there is a significant electron-mass enhancement due to the electron–phonon interaction. Since $\gamma_{exp} = \gamma_0(1 + \lambda)$, we can assess the electron-mass enhancement factor λ to be 0.82.

3.3. The static structural properties

The total energies are calculated as a function of cell volume. The Ewald correction [16] is added to the total energy. Because of the different sizes of the Wigner–Seitz spheres that we have chosen, the general form of the Ewald correction is used [17]. The total energy converges to better than 1 mRyd. For $LaIn_3$, we have neglected the La f orbital in the total energy calculation, since the La f states give only a minor contribution to the bonding of $LaIn_3$ (see table 1 and figure 2).

The calculated total energies for five values of the cell volume are fitted to a quadratic form to obtain the zero-temperature equilibrium lattice constant a_{eq} and bulk modulus B. The results are summarised in table 2 where they are compared with the experimental data [10, 18] and with the ASW calculation of $LaIn_3$ [7]. Our calculated lattice constants

are slightly smaller than the experimental values. This can partially be attributed to thermal expansion, since our results should correspond to the case of 0 K. The calculated bulk moduli indicate that bulk $LaIn_3$ is soft compared with bulk $LaSn_3$.

In summary , we have calculated the electronic band structures and the static structural properties of the rare-earth inter-metallic compounds $LaSn_3$ and $LaIn_3$. We have found that there are some differences between the electronic structure of LaM_3 and CeM_3. In LaM_3, the interactions between La d and M p electrons are predominant, which is the common character of transition-metal compounds, while in CeM_3, except for the interaction of Ce d and M p, the Ce 4f electrons have quite a large contribution to bonding. The La 4f states are localised states in LaM_3, but the Ce 4f states show an itinerant property which may be responsible in part for the mixed valence properties of CeM_3.

Acknowledgment

This work was supported by the National Science Foundation of the People's Republic of China.

References

[1] Toxen A M and Gambino R J 1968 *Phys. Lett.* **28**A 214
[2] Havinga E E 1968 *Phys. Lett.* **28**A 350
[3] Ye L, Huang M C and Zhu Z Z 1987 *Acta Phys. Sinica* **36** 981
[4] Gray D M and Meisel L V 1972 *Phys. Rev.* B **5** 1299, 1308
[5] Freeman A J and Koelling D D 1972 *J. Physique Coll.* **33** C3 57
[6] Koelling D D 1982 *Solid State Commun.* **43** 247
[7] Hackenbracht D and Kubler J 1979 *Z. Phys.* B **35** 27
[8] Koelling D D and Harmon B N 1977 *J. Phys. C: Solid State Phys.* **10** 3107
[9] Hedin L and Lundqvist B I 1971 *J. Phys. C: Solid State Phys.* **4** 2064
[10] Landelli A and Palenzona A 1979 *Handbook on the Physics and Chemistry of Rare Earths* vol 2 (Amsterdam: North-Holland)
[11] Chadi D J and Cohen M L 1973 *Phys. Rev.* B **8** 5747
[12] Toxen A M, Gambino R J and Welsh L B 1973 *Phys. Rev.* B **8** 90
[13] Bucher E, Andres K, Maita J P and Hull G W Jr 1968 *Helv. Phys. Acta* **41** 723
[14] Toxen A M, Gambino R J and Van der Hoeven B J C Jr 1971 *Proc. 12th Int. Low-Temperature Conf.* ed. E Kauda (Kyoto: Academy of Japan) p 351
[15] Umlauf E, Schmid W, Bredl C D, Steglich F and Loewenhaupt M 1979 *Z. Phys.* B **34** 65
[16] Esposito E, Carlsson A E, Ling D D, Ehrenreich H and Gelatt C D Jr 1980 *Phil. Mag.* A **41** 251
[17] Tang S P, Zhang K M and Xie X D 1988 *J. Phys. C: Solid State Phys.* **21** L777
[18] Stassis C, Zarestky J, Loong C K and McMasters D D 1981 *Phys. Rev.* B **23** 2227